Design and Performance Analysis of a Dual Band Patch Antenna and its MIMO Implementation for Wi-Fi, Radar, and V2X Applications

Prem Pal Singh[1], Sudhir Kumar Sharma[2], and Neetu Gupta[3]
[1]Department of Electrical Engineering, Modern Institute of Technology and Research Centre, Alwar, Rajasthan, India
[2] Department of Electronics and Communication Engineering, Jaipur National University, Jaipur, Rajasthan, India
[3] Department of Electronics and Communication Engineering, Jaipur National University, Jaipur, Rajasthan, India

Corresponding author: Prem Pal Singh (e-mail: ppsherpur.12392@ gmail.com).

ABSTRACT A dual-band 2-port Multiple Input Multiple Output (MIMO) antenna is designed and analyzed in this paper. The designed antenna resonates at two frequencies, 4.54 GHz and 5.8 GHz, with bandwidths of 340 and 360 MHz for each band, respectively. A low-cost FR-4 substrate with a dielectric constant of 4.4 and a thickness of 1.6 mm is used to simulate and fabricate the antenna. Total dimension of a single antenna element is 17 mm×22 mm×1.6 mm (0.25λ×0.32λ×0.024λ), and the MIMO configuration measures 45 mm×22 mm×1.6 mm (0.66λ×0.32λ×0.024λ) at 3.6 GHz. The fundamental parameters of MIMO antenna like isolation (>20dB), ECC (<0.00012), DG (~10), MEG (-3dB), CCL (<0.2 bps/Hz) and TARC (<0.3) and radiation parameters are evaluated which prove the practicality of the antenna for Wi-Fi (5.725-5.85 GHz), 5G applications in Japan (4.4-4.5 GHz), radar (civilian and military), amateur radio communications (5.65-5.925 GHz), and Vehicle-to-Everything (V2X) (5.85-5.925 GHz) communication systems. Also, the designed antenna demonstrates radiation efficiency of more than 69% across first operating band and more than 76% across second operating frequency. The designed antenna can also be used in remote sensing applications to study various environmental parameters at 4.54 GHz, as electromagnetic waves at this frequency penetrate easily and provide data on soil moisture, vegetation, etc.
INDEX TERMS MIMO Antenna, 5G, Dual Band, Wi-Fi, V2X.

I. INTRODUCTION

The demands for mobile communications has increased over the past years and single-band antennas are not appropriate for the current communication model because for multiple services multiple antennas are required that occupy more area, and it affects the performance of communication system [1-2]. In modern communication systems, multiband antennas are important because multiband services are embedded in a single antenna [1]. Multiband antennas reduce the size as well as the cost of the antenna system and help to enhance the functionality of the system. Also, with a single-antenna system, the transmission rate is low. For high data rates, increased efficiency, and reduced multipath fading effects MIMO antennas are a perfect choice. There are various challenges in designing high-isolation and compact antennas. When more than one antenna is placed together, it affects radiation characteristics of antenna because of mutual coupling. Therefore, it is important to reduce mutual coupling [2]. In addition to this, dual-band antenna with a MIMO configuration is difficult to design.

Previous findings were mainly focused on to reduce the mutual coupling between antennas of MIMO system by the application of different isolation structures [3-6]. In [3], to improve isolation, a C-shaped slot with a rectangular slot and a slit is etched in the ground plane. Antenna covers 2.34–2.71 GHz and 3.72–5.10 GHz bands which are designated for 5G applications. For the two-port antenna, the isolation is more than -20dB. Another 2-port antenna for a single 5G band is proposed in [4] operating from 3.25 to 3.85 GHz. To improve the isolation, truncated ground with stubs has been implemented. Also, a T-shaped stub is placed between radiating elements to further improve the isolation. A decagon-shaped antenna resonating on 3 bands is proposed in [5] and its MIMO configuration proposed by placing antenna elements orthogonally. Grounds are not connected, and no isolation structure is used. Another antenna structure which consists of multi slotted patch to get multiple bands, is presented in [6]. Without connecting the ground plane and using a defected ground structure mutual coupling is reduced in the 2-port MIMO configuration. A decoupling structure is placed between antenna elements to further improve the mutual coupling. This antenna is useful for S, C, and X band applications.

A 3-band 2-port MIMO Antenna array for WLAN applications resonating at 2.4, 3.0, and 5.8 GHz is implemented in [7]. For multiband operation, a CSRR is introduced in the ground plane to generate multiple resonances. The length and width of the MIMO configuration are 106.60 mm and 106.60 mm and overall, the antenna size is large. A prototype of the antenna was fabricated and validated experimentally. The isolation

achieved is more than -20 dB. The CSRR design is analyzed using mathematical equations. In [8], a Dual-band MIMO patch antenna with dimensions of 32×22 mm^2 operating at 5.9 and 7.7 GHz, making it suitable for WLAN and C-band applications. An asymmetrical coplanar strip (ACPS) and a combination of DGS and ACPS is used to increase the isolation. 2-port and 4-port antennas for operating in Sub-6 GHz 5G applications are proposed in [9-10] with isolation of more than -18 dB. The antenna in [9] provides an operating bandwidth from 3.25 to 3.85 GHz. A rectangular stub in the ground plane and two side stubs improve the isolation. Also, a T-shaped stub placed between the antenna elements enhances both bandwidth and isolation. For vehicle communication, it is important to recognize the driving environment automatically. For this purpose, patch antennas are proposed. Such an antenna is designed in [11], which is a C-shaped structure. The three frequencies can be controlled by adjusting the length of round shaped stubs. The three frequency bands are 2.4, 3.5, and 5.9 GHz. Various techniques to increase isolation and reduce mutual coupling to improve the performance of MIMO antennas are proposed and explained in the literature. Defected ground structure (DGS) is also a common and easy-to-design technique. Different multiband antennas, with and without MIMO configurations and with different mutual coupling reduction techniques are designed for different applications in [12-16]. MIMO antenna configuration for C, X-band, Wi-Fi/WiMax and wearable applications with dual and multiband operation are proposed in [18-23]. To reduce the mutual coupling between antenna elements, different decoupling structures are employed. Four triangular shaped antenna elements are placed parallelly and a cross shaped EBG and metamaterial structure is placed between them to mitigate the mutual coupling effect in [22].

In the current study, a dual-band 2-port MIMO Antenna with multi-segment radiating structures is proposed. Dual-band characteristics with resonances at 4.54 and 5.8 GHz are achieved. The initial stage of the design process includes design of a single antenna element. The purpose of designing the MIMO configuration of the antenna is to enable it for high data rate, high channel capacity, mitigation of interference, and prevention o fading. The geometry and design steps of the single-element antenna are presented in section II. Simulated and measured results of single element antenna and MIMO antenna are provided in sections III and IV. Finally, the paper is concluded in section V.

II. SINGLE ANTENNA CONFIGURATION

A. Antenna Element Design

The proposed dual-band antenna is designed with a multi-segment structure. The radiator of the antenna consists of various segments with a hook-shaped structure. The length of each segment was adjusted to achieve the desired frequency band using parametric analysis and the appropriate position of each segment was determined accordingly. A rectangular slot of length L_S and width W_S is introduced in the ground plane which create a sharp resonance in the lower band. Design and dimensional parameters of the proposed single-element antenna are shown in Figure 1. The FR-4 substrate is selected for simulation and fabrication purposes with ε_r=4.4 and thickness h=1.6 mm. The material used for radiating patch and ground plane is copper with trace thickness of 0.035 mm. The physical width W_{Sub} and Length L_{Sub} of the substrate are 17 mm and 22 mm respectively. The final physical dimensional parameters of the proposed single antenna element are summarized in Table I.

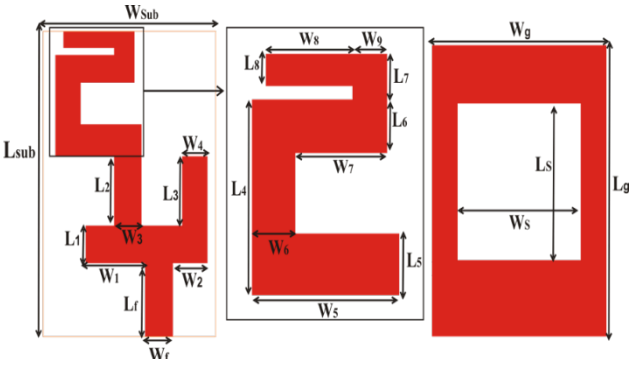

FIGURE 1. Dimensional Geometry of Antenna (a) Front View (Patch) (b) Back View (Ground Plane)

TABLE I. Dimensions of the Proposed Antenna

Parameter	Value(mm)	Parameter	Value(mm)
L_{Sub}	22	L_S	11.3
W_{Sub}=W_g	17	W_1	5.85
L_f	5.3	W_2	3.4
L_1= W_3	2.7	W_f	2.75
L_2	5	W_4= W_6	2.5
L_3	5	W_5	8.5
L_4	7.3	W_7	5.3
L_5	2.3	W_8	5
L_6	2	W_9	2
L_7	1.7	W_S	12
L_8	1.2	L_g	21

The operating frequency of the proposed antenna is obtained using Equation (1) [21]

$$L_{eg} = \frac{c}{4f_r\sqrt{\varepsilon_{reff}}} \quad (1)$$

Where c is the speed of light, f_r is the desired resonance frequency, L_{eg} represents the effective guided quarter wavelength of the desired frequency, ε_r is the dielectric constant of the substrate, ε_{reff} is the effective dielectric constant, calculated using equation (2) [21] and is approximately set to 2.32.

$$\varepsilon_{reff} = \sqrt{\varepsilon_r + 1} \quad (2)$$

$$\varepsilon_{reff} = \sqrt{4.4 + 1} = 2.32$$

L_{eg1} represents the effective guided quarter wavelength for frequency of 4.54 GHz, which can be calculated for the first operating frequency of 4.54 GHz as

$$L_{eg1} = \frac{\lambda_{eg1}}{4} = \frac{c}{4f_{r1}\sqrt{\varepsilon_{eff}}} \quad (3)$$

$L_{eg1} = \frac{3\times10^8}{4\times4.54\times10^9\sqrt{2.32}} = 10.83$ mm

Now based on the antenna geometry, effective electrical length of the antenna can be obtained by equation (3)

$L_{eg1} = W_1+W_2+W_f + L_3+L_4-(L_2+W_5)$ (4)

$L_{eg1} = 5.85+3.4+2.75+5+7.3-(5+8.5) = 10.8$ mm

The effective electrical length for the operating frequency of 4.54 derived from antenna geometry is nearly close to the effective guided quarter wavelength L_{eg1}.

L_{eg2} represents the effective guided quarter wavelength for the second operating frequency (f_{r2}) of 5.8 GHz. From equation (1), effective guided quarter wavelength for this frequency is

$$L_{eg2} = \frac{\lambda_{eg2}}{4} = \frac{c}{4f_{r2}\sqrt{\varepsilon_{eff}}}$$

$L_{eg2} = \frac{3\times10^8}{4\times5.8\times10^9\sqrt{2.32}} = 8.45$ mm

The effective electrical length for this frequency, derived from antenna geometry, is characterized by equation (5)

$L_{eg2} = (W_7+L_4) -(L_5+L_6)$ (5)

$L_{eg2} = (5.3+7.3) -(2.3+1.9) = 8.4$ mm

Therefore, the effective electrical length from antenna geometry is almost equal to the effective guided quarter wavelength evaluated using equation (1). The equations are derived from antenna geometry and then proved by simulation.

B. Parametric Analysis

Parametric studies are essential to examine the effect of key design parameters on the final antenna design and its performance. To perform a parametric analysis, the values of significant antenna parameters are varied, and their effects on the performance of the antenna are analyzed. This analysis helps to achieve the optimal values of the design parameters. This was performed using EM simulation software HFSS V.19. Parametric analysis helps to understand the shift in operating frequency and the variation in the value of reflection coefficients with the design parameters. The effect of variation in W_8, W_1, L_3 and L_S is studied. Different radiator structures can generate two frequencies and variations in the dimension of these radiators can shift the operating bands and can affect the return loss values. The effect of these parameters (W_8, L_3, L_3 and L_S) is displayed in figure 2(a), 2(b), 2(c), and 2(d) respectively. As evident from figure 2(a), the reflection coefficient varies with W_8 and the second frequency band shifts slightly. This shows that variation in W_8 shifts the second band from its center frequency. Similarly, variation in L_3 affects the reflection coefficient of the first frequency band. When the length L_S is varied from its optimal value then it shifts both bands slightly to the lower and upper side. It also affects the values of the reflection coefficients.

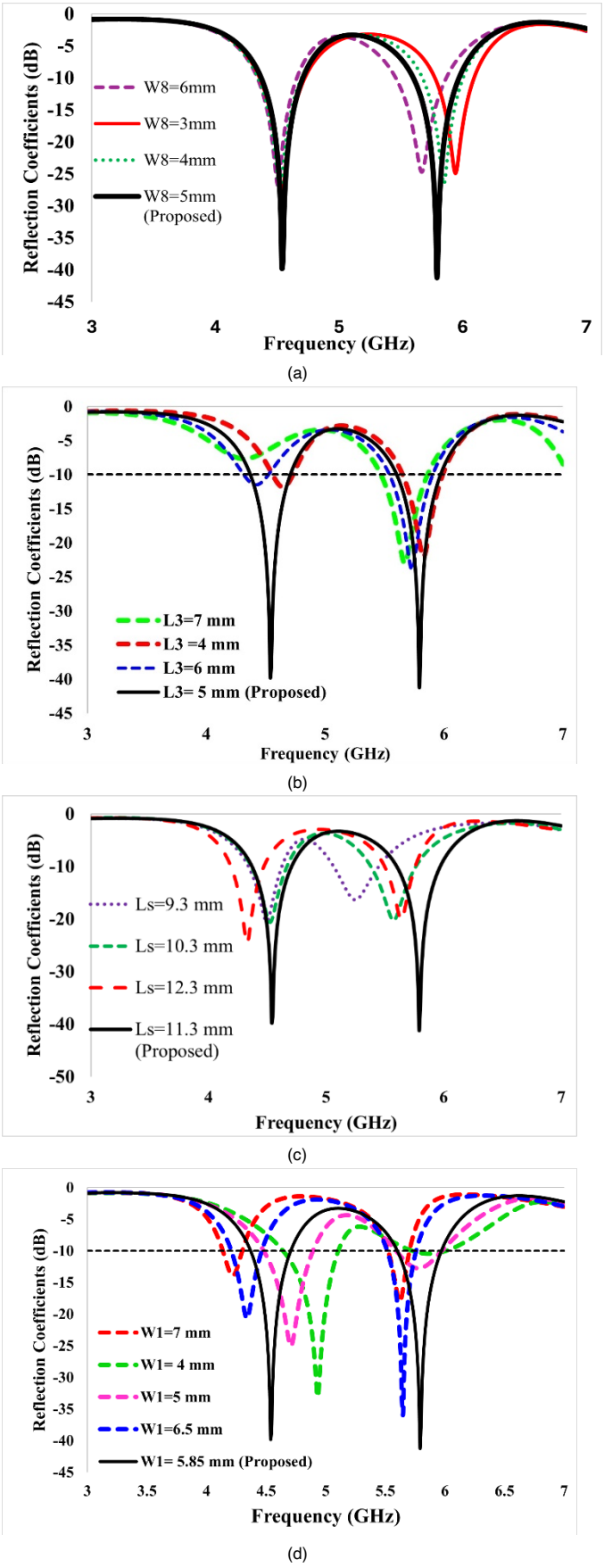

FIGURE 2. Reflection coefficient variation with (a) W_8 (b) L_3 and (c) L_S (d) W_1

Variation in horizontal length W_1 shifts the frequency of lower band from its center frequency. It also affects the values of reflection coefficients in both the bands. Figure 2(d) shows that the suitable value (5.85 mm) provides desired frequencies with good return loss.

C. Evolution of Proposed Antenna Element

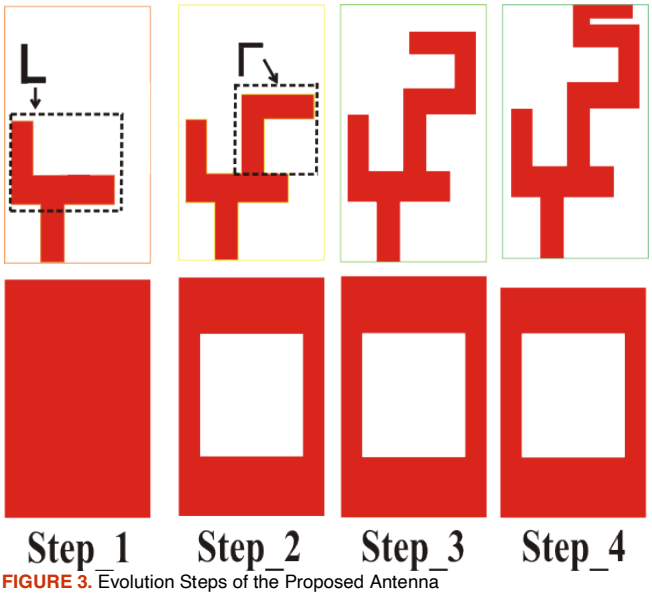

FIGURE 3. Evolution Steps of the Proposed Antenna

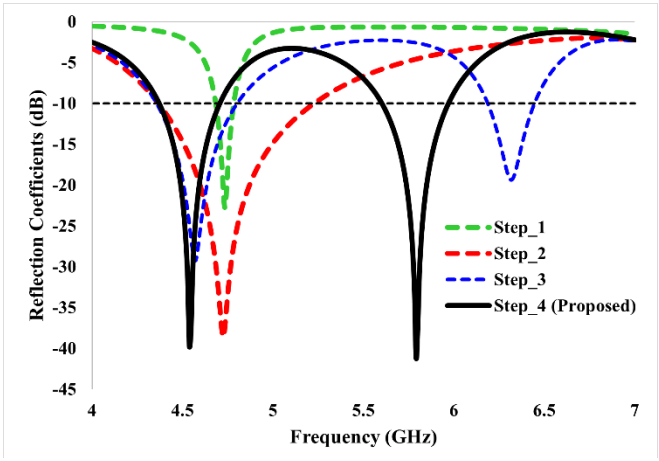

FIGURE 4. Return loss parameters of different design steps

TABLE II. Simulation Results of the Design Evolution

Step	F_r (GHz)	Operating Band (GHz)	Return Loss (dB) at F_r
Step-1	6.72	6.64-6.81	-13.97
Step-2	4.72	4.36-5.22	-38.60
Step-3	4.57, 6.31	4.36-4.79, 6.15-6.45	-29.29, -19.36
Step-4	4.54, 5.8	4.36-4.70,5.60-5.96	-39.68, -41.11

*F_r=Operating Frequency

To achieve the desired operating frequencies, the electrical length increases in incremental order. The proposed antenna is developed in four steps, which are illustrated in figure 3, and the corresponding S-parameters of all four steps are shown in figure 4. Additionally, the simulated results of all four steps in terms of operating frequency and return loss are summarized in Table II. The design of the proposed antenna initiated by designing an L-shaped radiator on the top side of substrate which is encircled in figure 3 and a full ground on bottom side.

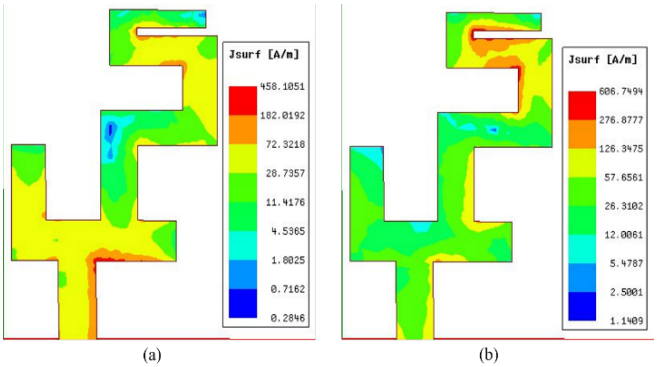

FIGURE 5. Current distribution at (a) 4.54 GHz (b) 5.8 GHz

This radiator fed with a 50 Ω microstrip line having vertical length of 5.3 mm and width of 2.75 mm. In this step, the antenna operates at 4.35-4.57 GHz frequency band. In step 2, a rectangular slot of dimensions 12 mm×11.3 mm is etched in the ground plane. Additionally, 'Γ-shaped' structure was added to the right side of feed line. This results in a better reflection coefficient for frequency band 4.36-5.22 GHz with center frequency of 4.72 GHz. The added structure increases the effective electrical length, but the slot in the ground plane results in a shift of the frequency to the lower side of the band (4.36-5.22 GHz). In step 3 of design process, another ٦-shaped structure was added to Γ-shaped structure resulting in a hook-shaped structure. As a result, the antenna operates at 4.36-4.80 GHz and 6.19-6.44 GHz frequency bands. The bandwidth of the lower band obtained in step 3 is reduced to 4.36-4.8 GHz. Resonance frequency also shifts to 4.54 GHz. Finally, in step 4, another 'Γ-shaped structure with vertical stub of 0.5 mm is connected. Additionally, some of the parameters of the final antenna were adjusted to achieve the desired results in terms of return loss and operating frequency. Length of the ground plane was reduced to 21 mm. the final antenna configuration was achieved through careful parametric analysis of radiator parameters, achieving dual band operation of 4.36-4.70 GHz and 5.60-5.96 GHz.

It has been observed that different segments of the antenna are responsible for different frequencies. The simulated results of different design steps are summarized in Table II. The simulated results in terms of return loss are illustrated in figure 4. The S11 parameters of step 4 indicate that the antenna efficiently operates in two bands, i.e., 4.36-4.70 GHz and 5.60-5.96 GHz, which align with the desired results.

The simulated surface current distribution of the antenna on both operating frequencies is shown in figure 5(a) and 5(b). It was found that the maximum current distribution at 4.54 GHz was concentrated near the feed line and horizontal strip connected to it. Additionally, the current was distributed to upper ' ┌' shaped strip. Similarly for the second operating frequency of 5.8 GHz, the maximum current is concentrated on the upper strips, as shown in figure 5(b). A small current was also observed on the feed line.

D. Results of Single Antenna

Figure 6 displays the fabricated prototype of the proposed antenna and the measurement setup for return loss using Keysight N9916A VNA.

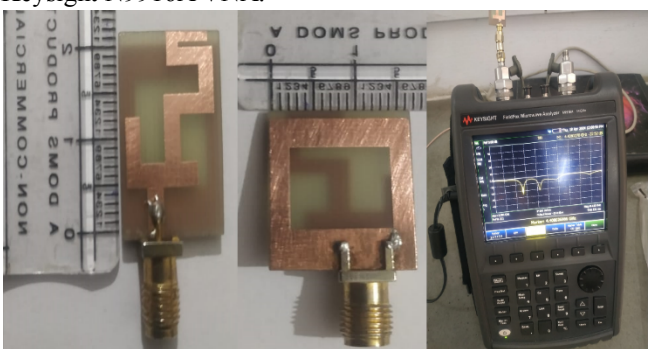

(a) (b) (c)

FIGURE 6. (a) Fabricated prototype of single antenna element (a) Front View (b) Back View (c) Measurement setup

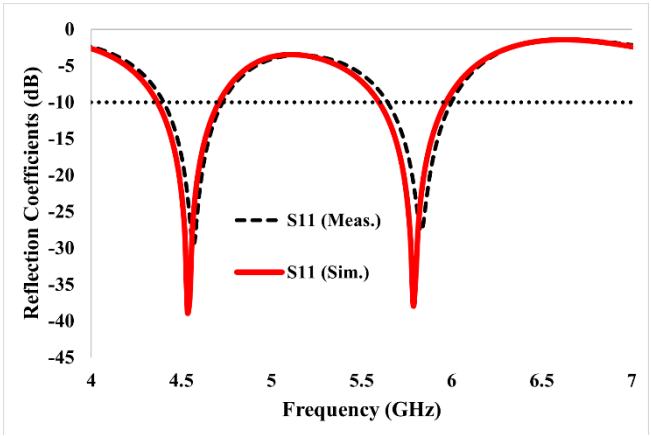

FIGURE 7. Simulated and Measured S-parameter response of single antenna element

The simulated and measured return loss parameters of the single antenna element are illustrated in figure 7. The small shift in the measured results could be possible because of soldering and fabrication process. The gain of the single antenna exceeds 3 dBi across both operating frequencies. At 4.54 and 5.8 GHz, the gain is observed to be 3.3 dBi and 3 dBi respectively. The gain plots for both operating frequencies are shown in figure 8.

III. MIMO ANTENNA CONFIGURATION

A. 2 Port Antenna Geometry

In section 2, the analysis of a single antenna element is carried out and, in this section, the two identical antenna elements (as in step-4) are arranged in a mirrored-image manner to implement 2-port antenna. Both the antenna elements are placed side by side with a of distance of D between them. On the bottom side of the substrate, two ground planes are placed and connected using a rectangular strip of length D_1. 2-Port antenna configuration is shown in figure 9. The fabricated prototype of the proposed antenna and the measurement setup on VNA are shown in figure 11.

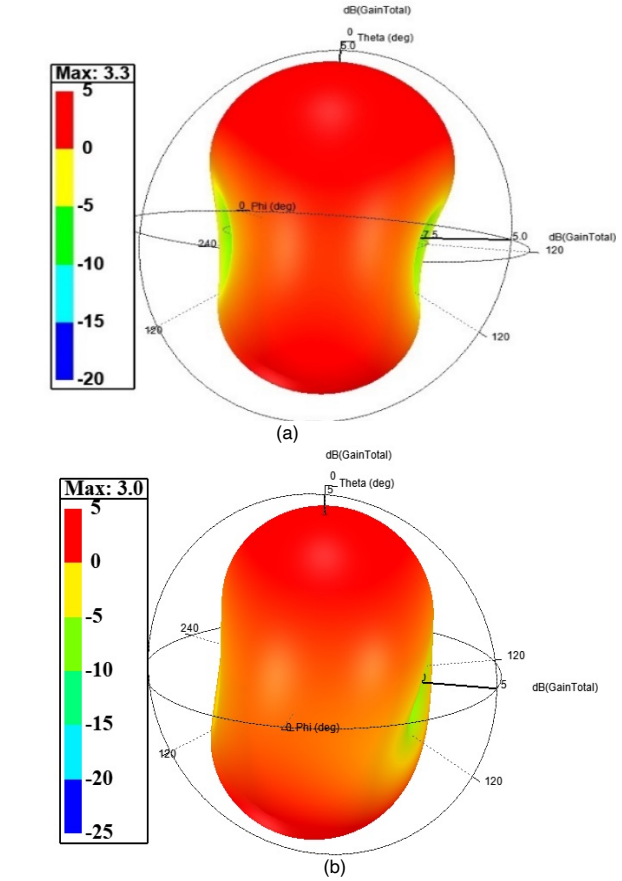

FIGURE 8. 3D Gain plot of single antenna element (Left side: at 4.54 GHz, Right side at 5.8 GHz)

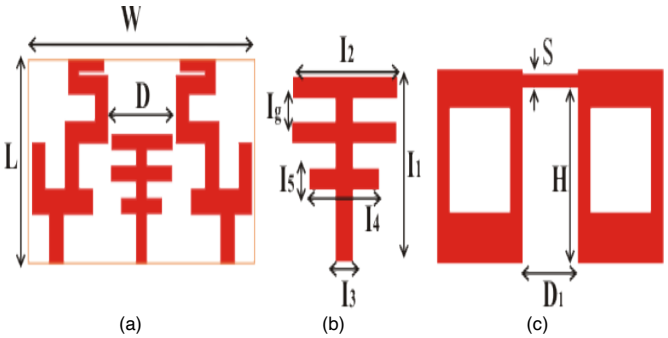

FIGURE 9. Geometry of 2-Port MIMO Antenna (a) Front View (b) Isolation Structure (c) Back View

Results obtained in terms of isolation with unconnected ground are good, but unconnected ground planes limit its real-system applications because there must be a common path or reference plane between all ground planes without affecting the performance of each antenna element [17]. In the literature, various techniques have been proposed by researchers to achieve maximum isolation between antenna elements but in this design a unique structure is used to mitigate mutual coupling between two antenna elements which consists of a vertical strip of length I_1 to which three horizontal strips are connected. This structure acts as a decoupler and supresses the surface currents that travel between the two antenna elements. The horizontal strips are placed at a gap of I_g. Without this structure, the antenna elements are not isolated efficiently which can be observed from figure 10(b).

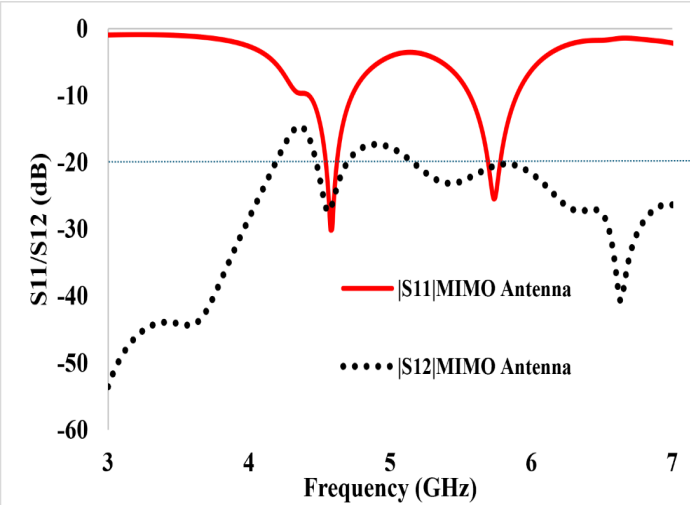

(a)

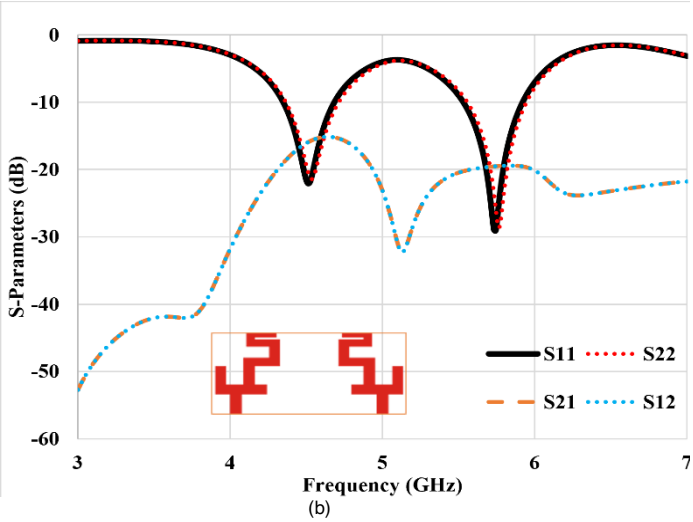

(b)

FIGURE 10. (a) Simulated S- Parameters of the proposed 2-Port MIMO antenna (b) S-Parameters of Antenna without Isolation structure

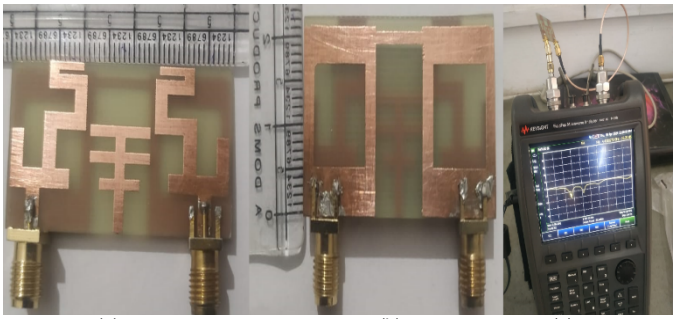

(a) (b) (c)

FIGURE 11. Fabricated Prototype of the MIMO Antenna (a) Front View (b) Bottom View

The mutual coupling can also be analyzed by current distribution shown in figure 12 at 4.54 GHz and 5.8 GHz with port 1 excited 1 and port 2 matched to a 50Ω load impedance. From current distribution, it is evident that the current is distributed maximum at port 1. Similarly, when port 2 is excited, the maximum current is distributed at port 2. This ensures that both the antenna elements are isolated from each other efficiently which is also verified by the simulated S_{11} and S_{12} plots in figure 13.

TABLE III. Comparison of Single and 2-element Antenna

Parameters	Single Element Antenna	2-Port MIMO Antenna
Frequency Range (GHz)	4.36-4.70, 5.60-5.96	4.40-4.73, 5.58-5.92
Bandwidth	340 MHz, 360 MHz	330, 340
% Bandwidth	7.50%, 6.22%	7.22%, 6%
Max. Gain (dBi)	3.3, 3.0	3.76, 3.26

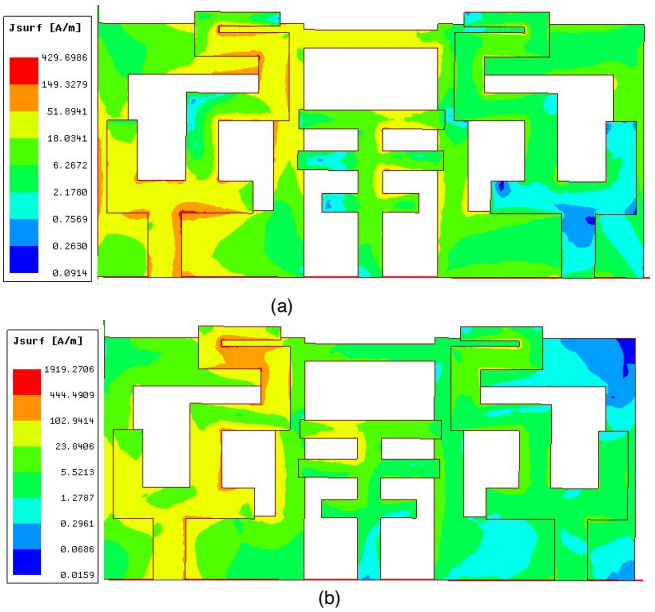

FIGURE 12. Current distribution of MIMO antenna at (a) 4.54 and (b) 5.8 GHz when port 1 is excited

Parameters of MIMO antenna are:- W=45 mm, L=22, D=3.6 mm, I_1=14 mm, I_2=12 mm, I_3=2 mm, I_4=8mm, I_5=1.6 mm, I_g=1.8 mm, S=1.5 mm, H=1 mm, D_1= 11mm.

The simulated and measured S_{11} and S_{12} of the antenna are shown in figure 13(b) which clearly indicates that the isolation within the frequency band 4.36-4.70 GHz and 5.60-5.96 GHz is more than 20 dB.

B. RESULTS AND DISCUSSION

i.Reflection and Transmission Coefficients

The simulated and measured S-parameters (S_{ii}, S_{ij} and S_{ji}) of the dual band 2-port antenna are plotted in figure 13. The simulated and measured -10 dB bandwidths for lower band are 340 MHz and 360 MHz. The simulated S_{11} for the first band is -30.04 dB and for the second band, it is -25.37 dB. The measured S_{11} values are -22.16 dB and -21.71 dB for the first and second bands, respectively. The measured S_{22} values are -25.60 and -22.43 dB for the frequencies 4.54 and 5.8 GHz, respectively. Slight difference is observed between simulated and measured S_{11} which is possible due to several losses such as copper and connector losses as well as error in fabrication.

From figure 13(b) it can be observed that the isolation between the two mirrored antenna elements is greater than 27 dB in the first band and greater than 20 dB in the second band.

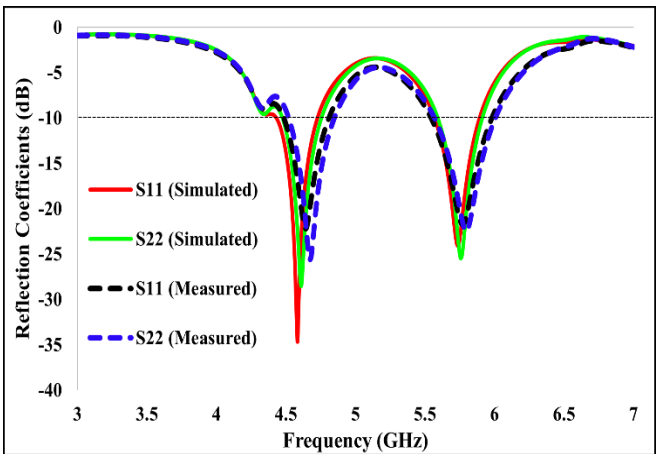

(a)

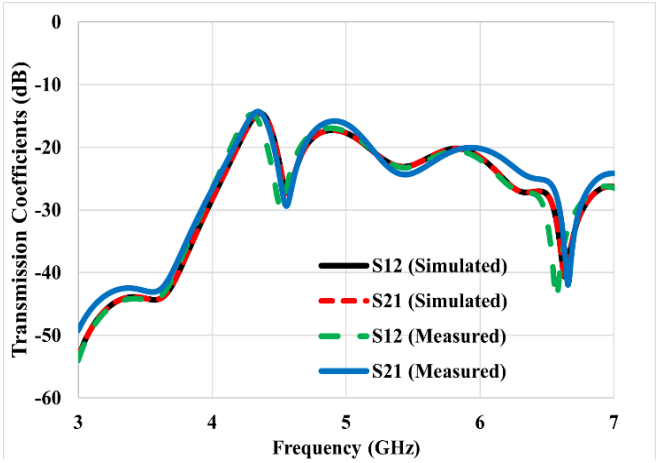

(b)

FIGURE 13. Simulated and measured (a) reflection and (b) transmission coefficients

Figure 14 illustrates the simulated and measured gain and radiation efficiency of the proposed MIMO antenna. The maximum gain obtained is 3.76 and 3.26 dBi at 4.54 and 5.8 GHz respectively. Figure 14 (b) shows the radiation efficiency of the Proposed antenna which is mostly above 68% in the first band and 75% in the second band.

ii.Radiation Performance

The measurement setup for measuring the radiation pattern is given in figure 15. Simulated and measured co-polar and cross polarization radiation patterns of both H-plane and E-plane are plotted in figure 16. If the orientation of receiver and transmitter antennas is same, then co-polar plots are observed, and cross polar plots are observed if the receiver and transmitter antennas are not in the same plane.

Proposed antenna is oriented in the XY plane, so the direction of radiation is along the Z-axis. In this configuration, $\phi=0^0$ corresponds to the XOZ plane and $\phi=90^0$ corresponds to YOZ plane. The radiation pattern of the antenna in $\phi=0^0$ and $\phi=90^0$ planes is illustrated in figure 16. According to figure 16(a), for $\phi=0^0$, at 4.54 and 5.8 GHz, the radiation pattern is omnidirectional and cross polarization is lower than co polarization which is an essential condition for ensuring that the antenna performs as intended.

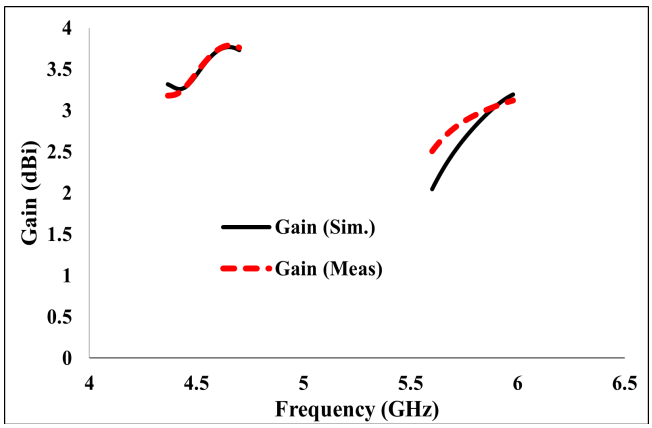

(a)

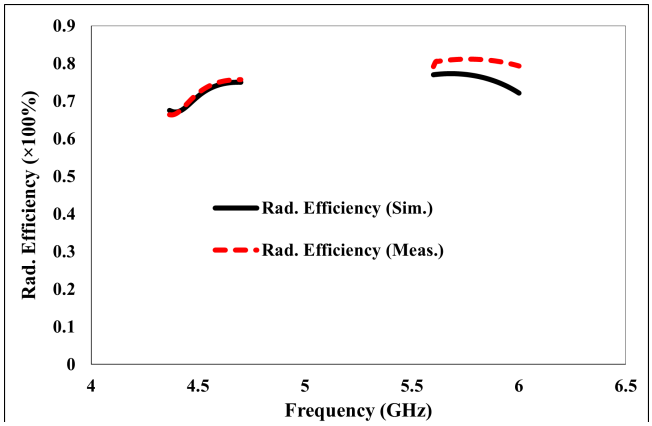

(b)

FIGURE 14. Simulated and Measured (a) Gain (b) Radiation Efficiency of 2-Port MIMO Antenna

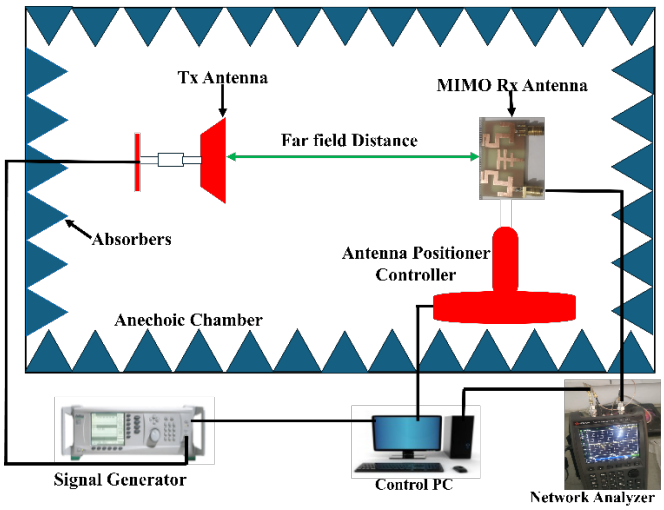

FIGURE 15. Radiation Pattern Measurement Setup

The antenna maintains low cross polarization, which is suitable in wireless applications that require wide coverage. For $\phi=90^0$, the radiation pattern is nearly bidirectional or shows a figure-eight shaped distribution and also the cross polarization is low, indicating the polarization purity as shown in figure 16(b). Thus, the omnidirectional pattern in the E-plane and the figure-eight shaped pattern in the H-plane are suitable for applications where broad coverage and reduced cross polarization are required.

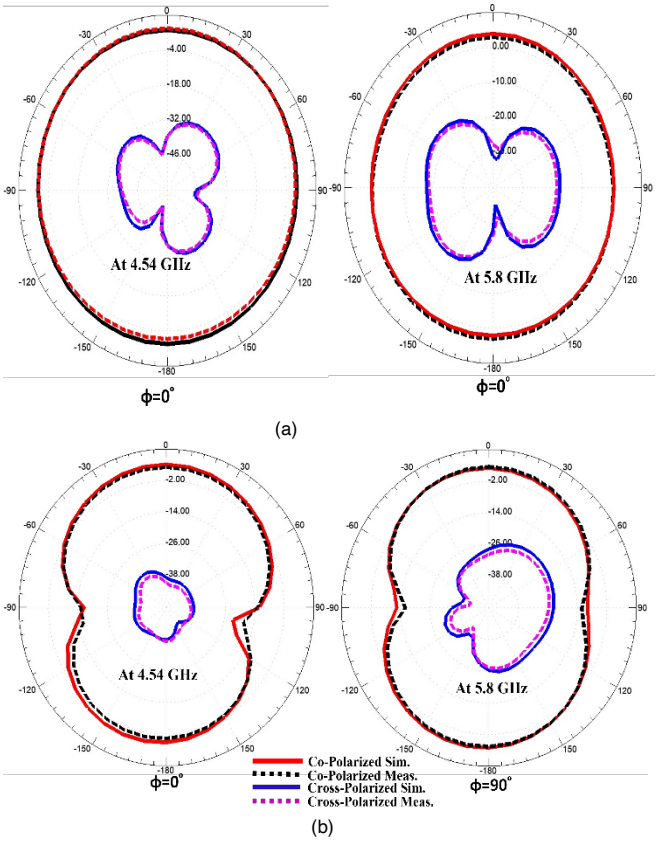

FIGURE 16. Simulated and measured co-pol and cross-pol radiation patterns of the MIMO antenna 4.54 GHz (b) 5.8 GHz

IV. MIMO PERFORMANCE PARAMETERS

When more than one antenna element is used, it is essential to analyze their diversity characteristics. This section evaluates and explains the diversity characteristics of the MIMO antenna which include the envelope correlation coefficient (ECC), diversity gain (DG) channel capacity loss (CCL), and mean effective gain (MEG), all of which are evaluated from simulated and measured S-parameters. Equations given in the literature are used to obtain these parameters.

A. ECC and DG

ECC helps quantify the channel quality by ensuring higher isolation with a lower ECC value. It shows how the emission from one antenna affects the others. Ideally the standard value of ECC is 0 but for 0.5 is acceptable value for practical applications [22]. The ECC value for the proposed antenna arrangement is <0.01 across both operating bands. ECC can be calculated from the scattering parameters using Equation (6) [18].

$$ECC = \frac{|S_{11}^{*}S_{12}+S_{21}^{*}S_{22}|}{(1-|S_{11}|^{2}-|S_{21}|^{2})(1-|S_{22}|^{2}-|S_{12}|^{2}} \quad (6)$$

Diversity gain (dB) can be obtained from ECC as ECC and DG are related to each other, as given in Equation (7). A diversity gain Value close to 10 dB is the threshold for better performance of the MIMO system. According to the literature, the DG (dB) should be equal to or nearly equal to 10 dB across the operating frequencies.

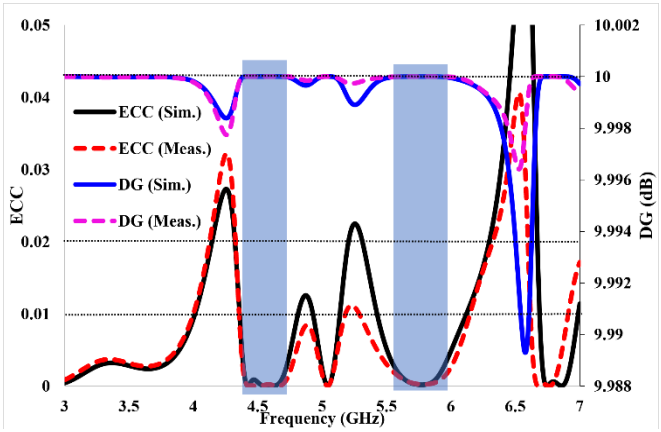

FIGURE 17. ECC and Diversity Gain (DG) of the Proposed

$$DG = 10 \times \sqrt{1 - |ECC|} \quad (7)$$

The diversity gain in the lower frequency band (4.36-4.70 GHz) is approximately 10 dB, fluctuating by only 0.001 dB, remains constant at 10 dB across the second band (5.60-5.96 GHz). These diversity parameters are obtained by exciting port 1 while keeping the second port connected with a 50Ω load impedance. The simulated ECC and DG (dB) calculated by using HFSS, along with the measured ECC and DG calculated from scattering parameters are plotted on the same graph, as displayed in figure 17. Both simulated and measured values of ECC and DG are within the acceptable range across both operating bands.

B. CCL, MEG and TARC

Channel capacity loss (CCL) is a critical parameter of MIMO antennas and following the literature, standard value for CCL is 0.4 bps/Hz [20]. For the proposed antenna, the CCL is found to be less than 0.2 bps/Hz across both the operating bands. The CCL of the MIMO antenna can be evaluated by using equation (8) [12] and the simulated and calculated CCL values, as shown in figure 18 are within the specified range.

$$CCL = -log\,(|\alpha^{R}|) \quad (8)$$

Where $\alpha^{R} = \begin{bmatrix} \alpha_{11} & \alpha_{12} \\ \alpha_{21} & \alpha_{22} \end{bmatrix}$

$\alpha_{ii} = (1 - |S_{11}|^{2} - |S_{21}|^{2})$ and $\alpha_{ij} = -(S_{ii}^{*}S_{ij} + S_{ji}^{*}S_{jj})$

for i, j=1 or 2

Another key parameter of a MIMO antenna is mean effective gain (MEG). Basically, it represents the gain performance of the MIMO antenna. In a fading environment, MEG represents the power received by the diversity antenna relative to the power received by an isotropic antenna [19]. The simulated and measured MEG between the two antenna elements at the operating frequency is nearly -3 dB indicating that the proposed antenna is suitable for the intended application. The ratio of MEG1 and MEG2 is also close to 0 dB, as shown in figure 19.

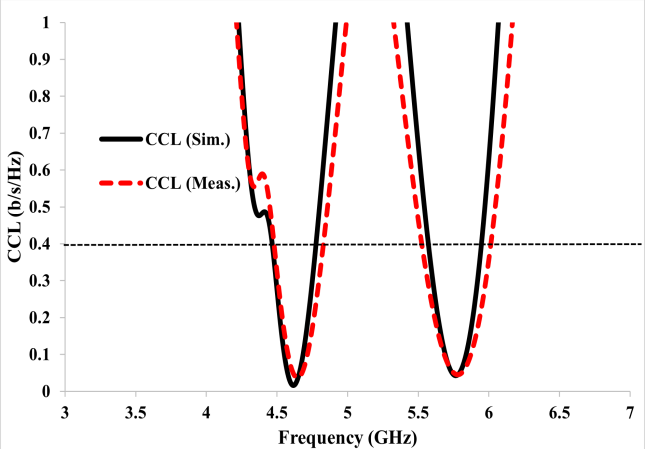

FIGURE 18. Simulated and Measured CCL of the Proposed Antenna

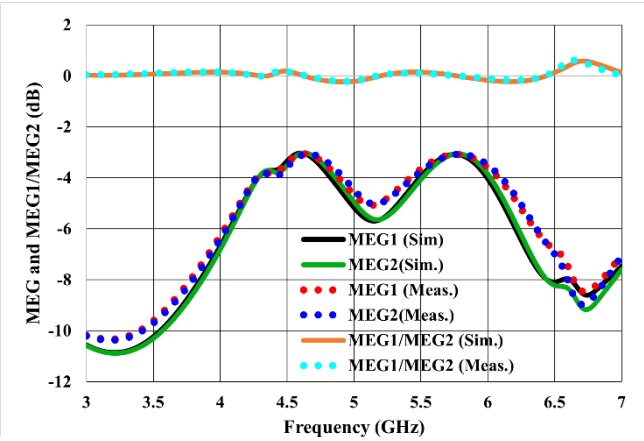

FIGURE 19. Mean Effective Gain of the MIMO Antenna

The MEG can be evaluated using the following equation can be used:

$$MEG_1 = 0.5[1 - |S_{11}|^2 - |S_{12}|^2] \quad (9)$$

$$MEG_2 = 0.5[1 - |S_{12}|^2 - |S_{22}|^2] \quad (10)$$

The degree of coupling and independence between two channels can be defined by TARC (Total Active Reflection Coefficient). It indicates overall reflection performance of a MIMO antenna. The standard value of TARC lies between 0 and 1 [4]. A value of 0 indicates that all the power is transmitted and 1 specifies that all the power is either reflected or diverted to other ports. A lower value of TARC indicates the better impedance matching.

TABLE IV. Summary of Diversity Performance of the MIMO Antenna

Operating Frequency (GHz)		Parameters				
		ECC	DG (dB)	MEG1, MEG2 (dB)	MEG1-MEG2 (dB)	CCL (b/s/Hz)
4.54	Sim.	0.00012	9.97	3.12, 3.10	0.1270	0.1343
	Meas.	0.00015	9.95	3.23, 3.36	0.1308	0.1926
5.8	Sim.	0.0002	9.95	3.20, 3.11	0.0364	0.0477
	Meas.	0.00024	9.96	3.09, 3.07	0.0125	0.0562

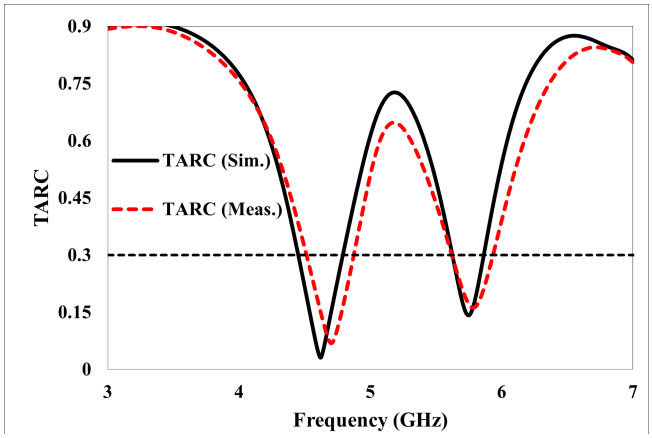

FIGURE 20. Simulated TARC of the Proposed Antenna

Figure 20 illustrates the simulated and measured TARC and it is observed to be below 0.3 in both operational bands. The simulated and calculated parameters, such as ECC, DG, MEG, and CCL of the MIMO antenna are summarized in Table IV.

C. Performance Comparison with Other Dual-band Antennas:

The proposed MIMO antenna is compared with previously designed antennas reported in literature in terms of size, bandwidth, gain and their limitations as summarized in table V.

TABLE V. Comparison with Existing 2-Port MIMO Antennas

Ref.	Dimensions (No. of Ports)	Band (GHz)	Max. Gain (dBi)	ECC and DG	CCL and MEG
2	30×26 mm^2 (2-Port)	Dual Band, 3.2-3.8, 5.7-6.2	2.8	0.03, >9.8	Not Given
5	23.5×83 mm^2 (2- Port) 70.5×83 mm^2 (4-Port)	Multiband	NA	<0.001, ~10	<0.4, <-3 dB
6	34×20 mm^2 (2-Port)	Multiband	2.9	<0.02, 9.99	~0.2, NA
7	106.6×106.6 mm^2 (4-Port)	3-band	4.3	<0.01, >9.98	NA, <3 dB
9	20×31.5 mm^2 (2 Port)	Single band (3.25-3.85)	NA	0.011, 10	0.3016, 0.48
18	120×120 mm^2 (2 Port)	Dual Band 4.23-4.55, 6.30-10.22	5.73	0.001, 9.99	Not Given
22	60×44 mm^2 (4-Port)	Single band 5-6.60	8	0.05, 9.7	NA
23	45×30 mm^2 (2-Port)	Dual band 2.40-2.57, 3.85-6.96	2.65	0.02, 9.98	NA
Prop. Work	22×45 mm^2 (2 Port)	Dual Band 4.36-4.70, 5.60-5.96	3.7	0.0001, ~10	<0.1, ~3 dB

Previously reported antennas occupied large area, exhibited small bandwidth and low gain. Although, the antenna in [6] is smaller in size than the proposed antenna but the gain is low and the isolation across two operating bands is less than 15 dB. Additionally, in most of the antennas the ground planes are not connected to each other, which limits their real system applications. The proposed antenna exhibits small

dimensions, sufficient gain, and grounds planes are connected due to which the antenna is useful for real systems applications.

V. CONCLUSION

A dual-band 2-port MIMO antenna of compact size has been designed, fabricated and analyzed in this study that operates at 4.36-4.70 GHz and 5.60-5.96 GHz frequency bands. An impedance bandwidth of 340 MHz and 360 MHz has been achieved for the two bands. The simulated and measured results are in good agreement for the desired frequency bands. A novel decoupling structure has been designed and used to improve the isolation between antenna elements at both the frequency bands additionally, the ground planes are connected. All the diversity parameters such as ECC, DG, CCL, TARC and MEG are evaluated, and all are within the acceptable range which satisfying all the requirements of a MIMO antenna and ensuring the suitability of the proposed antenna for different wireless applications, including Wi-Fi, mid band 5G, Vehicle-to-everything (V2X) communication and remote sensing. The proposed antenna can be extended to 4 or more ports in the future to enhance its diversity performance. Additionally, the antenna can be integrated with more efficient frequency selective surface (FSS), which can improve the gain and other parameters.

ACKNOWLEDGMENT

We would like to thank the Modern Institute of Technology and research centre Alwar, for providing the facilities to conduct this research, and thanks to SKIT Jaipur for offering the testing facility.

REFERENCES

[1] Mushtaq, M. T., Shah, S. M. A., Munir, S., Hussain, M., Iqbal, J., & Khan, U. H., "Dual Band Microstrip Semicircular Slot Patch Antenna for WLAN and WIMAX Applications", *Radioengineering*, Vol. *31*, No. 3, pp. 406–412, 2022. https://doi.org/10.13164/RE.2022.0406.

[2] Nirmal, P. C., Nandgaonkar, A., Nalbalwar, S., & Gupta, R. K., "*A Compact Dual Band MIMO Antenna with Improved Isolation for WI-MAX and WLAN Applications", Progress in Electromagnetics Research M, Vol. 68, pp. 69–77, 2018*.

[3] Xi, S., Cai, J., Shen, L., Li, Q., & Liu, G., "Dual-Band MIMO Antenna with Enhanced Isolation for 5G NR Application", *Micromachines*, Vol. *14*, No. 1, 2023. https://doi.org/10.3390/mi14010095

[4] Kumar, P., Singh, A. K., Kumar, R., Sinha, R., Mahto, S. K., Choubey, A., & Al-Gburi, A. J. A. (2024). High Isolated Defected Ground Structure Based Elliptical Shape Dual Element MIMO Antenna for S-Band Applications. *Progress In Electromagnetics Research C*, Vol. *143*, pp. 67–74, 2024. https://doi.org/10.2528/PIERC24031304

[5] Dileepan, D., Natarajan, S., & Rajkumar, R., "A High Isolation Multiband MIMO Antenna without Decoupling Structure for WLAN/WiMAX/5G Applications", In *Progress In Electromagnetics Research C*, Vol. 112, 2021.

[6] Rao, P. S., Babu, K. J., & Prasad, A. M. (2021). A Multi-band Multi-slot MIMO Antenna with Enhanced Isolation. *Wireless Personal Communications*, Vol. *119*, No. 3, 2239–2252, 2021. https://doi.org/10.1007/s11277-021-08328-z

[7] Aminu-Baba, M., Rahim, M. K. A., Zubir, F., Iliyasu, A. Y., Jahun, K. I., Yusoff, M. F. M., Gajibo, M. M., Pramudita, A. A., & Lin, I. K. C., "A compact triband miniaturized MIMO antenna for WLAN applications", *AEU - International Journal of Electronics and Communications*, Vol. *136, 2021.* https://doi.org/10.1016/j.aeue.2021.153767

[8] Pasumarthi, S. R., Kamili, J. B., & Avala, M. P., "Design of dual band MIMO antenna with improved isolation", *Microwave and Optical Technology Letters*, Vol. *61, No.* 6, 2019. 1579–1583. https://doi.org/10.1002/mop.31832

[9] Srinubabu, M., & Venkata Rajasekhar, N., "A compact and efficiently designed two-port MIMO antenna for N78/48 5G applications", *Heliyon*, Vol. *10, No.* 7, 2024. https://doi.org/10.1016/j.heliyon.2024.e28981

[10] Ren, Z., & Zhao, A., "Dual-Band MIMO Antenna with Compact Self-Decoupled Antenna Pairs for 5G Mobile Applications", *IEEE Access*, Vol. *7*, pp. 82288–82296, 2019. https://doi.org/10.1109/ACCESS.2019.2923666

[11] Woo, D. S., "A Triple Band C-Shape Monopole Antenna for Vehicle Communication Application", *Progress In Electromagnetics Research C*, Vol. 121, 2022.

[12] Armghan, A., Patel, S. K., Lavadiya, S., Qamar, S., Alsharari, M., Daher, M. G., Althuwayb, A. A., Alenezi, F., & Aliqab, K., "Design and Fabrication of Compact, Multiband, High Gain, High Isolation, Metamaterial-Based MIMO Antennas for Wireless Communication Systems" *Micromachines*, Vol. *14*No. 2, 2023. https://doi.org/10.3390/mi14020357

[13] Verulkar, S., Khade, A., Trimukhe, M., & Gupta, R. K., "Dual Band Split Ring Monopole Antenna Structures for 5G and WLAN Applications", *Progress In Electromagnetics Research C*, Vol. 122, 2022.

[14] Zhai, H., Gao, Q., Ma, Z., & Liang, C., "Dual Y-shaped monopole antenna for dual-band WLAN/WiMAX operations" *International Journal of Antennas and Propagation*, *2014*. https://doi.org/10.1155/2014/481918.

[15] Agarwal, M., Dhanoa, J. K., "Two-port hexagon shaped MIMO microstrip antenna for UWB applications integrated with double stop bands for WiMax and WLAN", *AEU - International Journal of Electronics and Communications*, Vol. *138*, 2021. https://doi.org/10.1016/j.aeue.2021.153885

[16] Verulkar, S., Rochkari, A., Trimukhe, M., Bodade, V., & Gupta, R., "High Gain Compact Dual Band Antenna Using Frequency Selective Surface for 5G and WLAN Applications", *Progress In Electromagnetics Research C*, Vol. *142*, pp. 1–11, 2024 https://doi.org/10.2528/PIERC24010101

[17] Sharawi, M. S. "Current Misuses and Future Prospects for Printed Multiple-Input, Multiple-Output Antenna Systems [Wireless Corner]", *IEEE Antennas and Propagation Magazine*, Vol. *59*, No. 2, pp. 162–170, 2017.https://doi.org/10.1109/MAP.2017.2658346.

[18] Bhalavi, B. S., Kumar, A., & Shrivastava, A., "Interconnected Ground Plane Structure Based High Isolation, Dual Band Quad-Element MIMO Antenna for C-Band, and X-Band Applications" Progress In Electromagnetics Research M, Vol. 127, pp. 131–139, 2024. https://doi.org/10.2528/PIERM24030606

[19] Khan, A. A., Jamaluddin, M. H., Aqeel, S., Nasir, J., Kazim, J. U. R., & Owais, O., "Dual-band MIMO dielectric resonator antenna for WiMAX/WLAN applications", *IET Microwaves, Antennas and Propagation*, Vol. *11,* No. 1, pp. 113–120, 2017. https://doi.org/10.1049/iet-map.2015.0745

[20] Shariff B. G, P., Naik, A. A., Ali, T., Mane, P. R., David, R. M., Pathan, S., & Anguera, J., "High-Isolation Wide-Band Four-Element MIMO Antenna Covering Ka-Band for 5G Wireless Applications", *IEEE Access*, Vol. *11*, pp. 123030–123046, Nov. 2023. https://doi.org/10.1109/ACCESS.2023.3328777

[21] Lin, C.-K.; Lin, D.-B.; Lin, H.-C.; Lin, C.-C, "Design of a Compact Multiband Monopole Antenna with MIMO Mutual Coupling Reduction", Sensors, Vol. 24, 2024, 5495. https://doi.org/10.3390/s24175495

[22] Althuwayb, A. A., Alibakhshikenari, M., Virdee, B. S., Rashid, N., Kaaniche, K., Atitallah, A. ben, Armghan, A., Elhamrawy, O. I., See, C. H., & Falcone, F., "Metasurface-Inspired Flexible Wearable MIMO Antenna Array for Wireless Body Area Network Applications and Biomedical Telemetry Devices," in *IEEE Access*, vol. 11, pp. 1039-1056, 2023, doi: 10.1109/ACCESS.2022.3233388.

[23] C. -Y. -D. Sim, V. Dhasarathan, T. K. Tran, J. Kulkarni, B. A. Garner and Y. Li, "Mutual Coupling Reduction in Dual-Band MIMO Antenna Using Parasitic Dollar-Shaped Structure for Modern Wireless Communication," in *IEEE Access*, vol. 11, pp. 5617-5628, 2023, doi: 10.1109/ACCESS.2023.3235761.